Check for updates

High Power Laser Science and Engineering, (2026), Vol. 14, e25, 8 pages.
doi:10.1017/hpl.2026.10120

HIGH POWER LASER SCIENCE AND ENGINEERING

RESEARCH ARTICLE

Power scaling of a fundamental-mode thin-disk laser using a gain-enhanced soft-aperture resonator

Renchong Lv[1,2], Huang Zhou[1], Sen Tian[1], Peng He[1], Jiangfan Pan[1], Lei Feng[1], Yong Zhen[1,3], Jiangfeng Zhu[3], Wenlong Tian[3], Xinkui He[1,2], and Zhiyi Wei[1,2]

[1]*Advanced Attosecond Laser Infrastructure (AALI), Songshan Lake Materials Laboratory, Dongguan, China*

[2]*Institute of Physics, Chinese Academy of Sciences, Beijing, China*

[3]*School of Optoelectronic Engineering, Xidian University, Xi'an, China*

(Received 8 December 2025; revised 20 January 2026; accepted 6 February 2026)

Abstract

We present a novel, compact resonator design for large-mode thin-disk lasers, producing 300 W average output power at a 1-kHz repetition rate within a cavity length of less than 5 m. High beam quality with $M^2_x = 1.06$ and $M^2_y = 1.15$ is achieved by breaking conventional mode-matching ratios and fully exploiting the disk's soft-aperture effect. In this work, an ytterbium-doped yttrium aluminum garnet thin-disk resonator is shown to produce fundamental transverse mode lasing with a mode size approaching or surpassing the pump spot dimension. Theoretical analysis demonstrates that the proposed cavity configuration enables a thin-disk regenerative amplifier to deliver pulse energy exceeding 200 mJ at 1 kHz repetition rate with excellent beam quality.

Keywords: fundamental mode; high power; soft aperture; thin-disk laser

1. Introduction

High-average-power, high-energy ultrafast laser sources find widespread applications in research and industry, encompassing attosecond science[1], extreme ultraviolet lithography[2] and advanced material processing[3,4], and are ideal pump sources for optical parametric chirped-pulse amplification (OPCPA) systems[5,6]. The demand required for pump lasers in these applications is commonly met by ultrafast laser systems based on slab, fiber or thin-disk laser gain geometrics. Among them, the thin-disk laser provides extremely efficient heat dissipation along the axis of the disk owing to its gain medium – the disk-shaped structure with a thickness of typically around 100 μm that operates as an active mirror[7,8]. In addition, the short propagation length within the gain medium significantly suppresses optical nonlinearities. Consequently, thin-disk technology has positioned itself as the leading platform for laser power and energy scaling. Systems based on this architecture have demonstrated an average power reaching up to 2 kW[9]and pulse energy as high as 720 mJ at a 1 kHz repetition rate[10]. However, the complexity and beam degradation inherent to multi-pass amplifiers make the power and energy scaling with oscillators or regenerative amplifiers particularly appealing[11–14]. The power and energy scaling of thin-disk lasers is usually achieved by simultaneously increasing the radii of the pump spot and laser mode on the thin disk while keeping the ratio of the radii constant; empirically, the optimal mode-to-pump ratio (MPR) has been found to be around 70%–80%[15–17]. Moreover, employing an active multi-pass cavity design[18] or cascaded thin disks[19] within the resonator significantly increases the small signal gain per round trip, enabling high-power operation. Currently, the oscillators providing near-diffraction-limited beam quality achieve up to 550 W in mode-locked operation[13]. As for regenerative amplifiers, 1 kW of output power at 5 and 10 kHz repetition rates was realized in 2017[19]. A thin-disk laser delivering pulse energy of 550 mJ at 1 kHz repetition rate was realized by Pfaff *et al.*[20] from Trumpf in 2021, which marked a significant milestone. Although existing results confirm exceptional high-power/energy capabilities in thin-disk lasers, such performance generally incurs longer cavity

Correspondence to: H. Zhou and Z. Wei, Advanced Attosecond Laser Infrastructure (AALI), Songshan Lake Materials Laboratory, Dongguan 523770, China. Emails: huang.zhou@outlook.com (H. Zhou), zywei@iphy.ac.cn (Z. Wei)

© The Author(s), 2026. Published by Cambridge University Press in association with Chinese Laser Press. This is an Open Access article, distributed under the terms of the Creative Commons Attribution licence (https://creativecommons.org/licenses/by/4.0), which permits unrestricted re-use, distribution and reproduction, provided the original article is properly cited.

https://doi.org/10.1017/hpl.2026.10120 Published online by Cambridge University Press

lengths, more components, greater design complexity[21] and intensive demand on the environment.

The aforementioned trade-off is mainly because the thin-disk resonators are often designed with a steady resonator, which ensures that the thin-disk crystal operates in a stable region across the entire power scaling range, especially for large-mode resonators[22]. From a laser dynamic perspective, large transverse modes are based on the balance of two quite weak counteracting effects: diffraction tends to enlarge the beam cross-section, while focusing effects on isolated optical elements. Expansion of the laser mode inevitably leads to a weaker diffraction effect. That means that the applied focusing effect also needs to be made correspondingly weaker, for example, by using only weakly curved laser mirrors, which requires a typically larger resonator length. Moreover, any additional effects can easily become substantial, such as misalignment of laser mirrors or any optical aberrations[23,24]. It is well known that one of the key considerations when designing thin-disk cavities is the influence of the thermal lens of the disk on the cavity mode evolution[25]. Thermal-induced parabolic phase profiles and non-parabolic terms need to be included in the design so that the cavity is optimized for operation at high power without beam quality degradation[26]. Collectively, these factors increase the complexity of large-volume-mode cavity designs, hindering industrial deployment and practical laser implementation. While recent efforts have focused on optimizing compact thin-disk laser cavities[27–29], fundamental-mode output power remains confined below the 100-W level.

In this paper, we present a significant achievement in large-mode area thin-disk laser resonator design, the gain-enhanced soft-aperture resonator (GESAR), achieving 300 W fundamental-mode output with near-diffraction-limited beam quality in a compact cavity with cavity length below 5 m. This result is made possible by combining several advancements in resonator architecture. Firstly, two cascaded disks pumped by a ZPL (zero-photon line)[30] 969 nm laser diode were used, decreasing thermal loading at each thin-disk crystal to alleviate thermal distortion effects. Secondly, the primary advantage of this method lies in its self-induced soft aperture for mode cleaning. The pump spot defines a gain region while the unpumped area introduces loss, which acts as soft aperture, effectively filtering higher-order modes and favoring TEM_{00} operation. In the GESAR configuration, the laser mode size on one disk falls within 70%–80% of the pump spot size consistent with conventional mode-matching requirements. This rule is deliberately exceeded in the second disk, where an increased spot size ratio fully exploits the gain-induced soft aperture's mode-filtering capability inherent to the gain medium, significantly improving higher-order mode suppression and guaranteeing stable single-transverse-mode operation. Combining theoretical modeling and experimental validation, we establish that this synergistic approach enables efficient, diffraction-limited operation with exceptional stability in the thin-disk resonator.

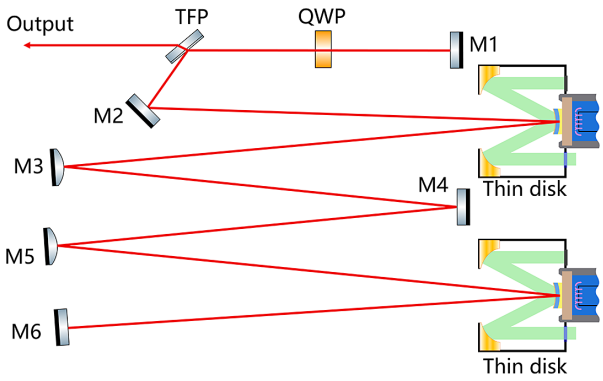


Figure 1. Schematic of the thin-disk laser resonator. QWP, quarter-wave plate; TFP, thin-film polarizer; M1–M6, mirrors.

2. Thin-disk resonator

2.1. Experimental setup

A schematic of the experimental GESAR setup is shown in Figure 1. The laser resonator consists of two custom-designed thin-disk modules, each with an ytterbium-doped yttrium aluminum garnet (Yb:YAG) thin disk bonded to a water-cooled diamond substrate. The disks have a thickness of 175 μm, a diameter of 12 mm and a doping concentration of 10% (atomic fraction). The nominal initial radii of curvature of the disks are –4.5 m without pumping. Each module is pumped by a wavelength-locked, fiber-coupled 969-nm laser diode delivering a maximum peak power of 1200 W, where the pump light is imaged 16 times onto the disk via a pump head, thereby ensuring an extremely high pump absorption efficiency after 32 pump beam passes through the disk. By using appropriate magnification optics, the pump spot diameter on the disk is maintained at 4.6 mm, exhibiting near-flat-top intensity distribution. Two cameras are used to monitor beam positions on the disks. In order to simultaneously mitigate the thermal load on the crystal and enhance laser efficiency, the laser diodes are operated in quasi-continuous-wave (QCW) mode at a 1 kHz repetition rate with 30% duty cycle. A tunable-coupling-rate output coupler, comprising a quarter-wave plate (QWP) and a thin-film polarizer (TFP), is employed to obtain maximum output. The whole system operates at room temperature and under atmospheric pressure.

2.2. GESAR design and simulation

As shown in Figure 1, the cavity consisting of two thin disks is in linear configuration with a total optical path length of 4.9 m. We engineered the Gaussian beam propagation on the

https://doi.org/10.1017/hpl.2026.10120 Published online by Cambridge University Press

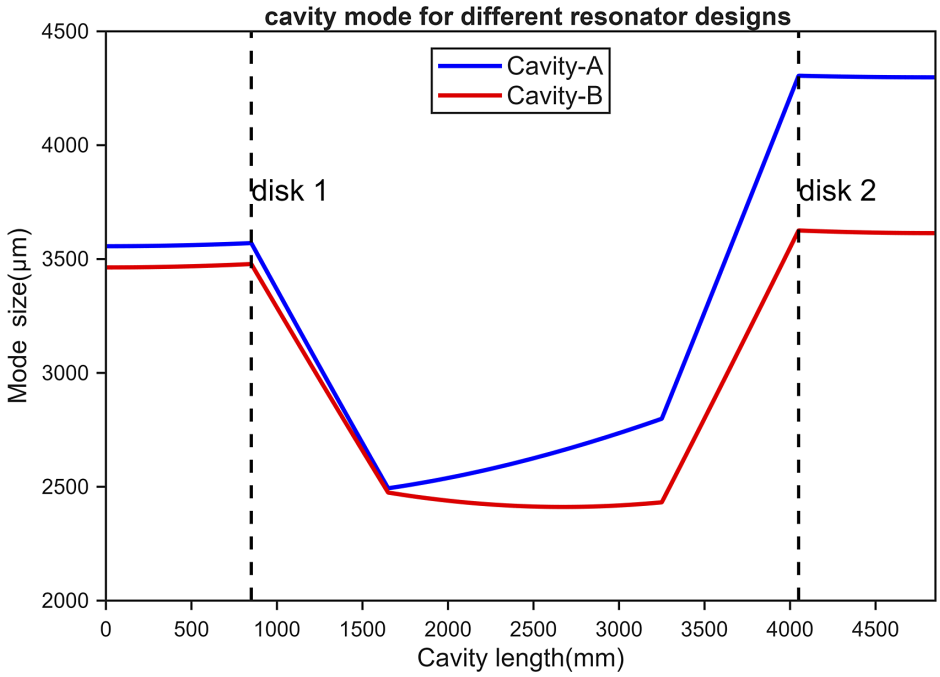


Figure 2. The laser mode radius evolution throughout the cavity is shown. The GESAR cavity mode is shown in blue, with cavity modes for the conventional cavity depicted in red.

thin disk within this resonator as a Fourier transform process to mitigate the impact of thermal lensing on cavity stability. Using ray transfer matrix simulation, the mode size evolution inside the cavity can be initially characterized. The cavity is designed such that the intracavity laser mode diameter is 3.6 mm ($1/e^2$) on disk 1. The corresponding MPR is 78%, which lies within the usual 70%–80% range that has been confirmed experimentally and numerically to yield good performance with near-diffraction-limited output and efficient energy extraction[16]. Conversely, on disk 2, the laser mode diameter is designed to be 4.4 mm with a larger MPR of 96%. For comparison, a conventional resonator utilizing the standard MPR of 70%–80% on both disks was constructed and is shown as Cavity B in Figure 2, while the GESAR is denoted as Cavity A. Figure 2 compares the variation of the intracavity mode size between the two resonator designs. Specifically, on disk 2, Cavity A demonstrates a significantly larger fundamental-mode spot size compared to Cavity B. For fundamental-mode operation of thin-disk lasers, it is generally understood that higher-order mode operation should be avoided. Such modes can be excited due to aberrations and resonances; thus, it is important to investigate the beam quality affecting factors closely. The ray transfer matrix formalism for Gaussian beam propagation is typically employed to model the parabolic phase profiles resulting from the thermal lensing effects of the disk. To quantify the influences of non-parabolic terms, a numerical spatially resolved model is applied[26]. The model employs the angular spectrum method to compute the evolution of the intracavity laser mode distribution. This simulation calculates the stable electric field distribution within the optical resonator by iteratively propagating the field inside the cavity until the distribution converges. A step-by-step calculation method is used, where each optical element is defined by its reflectivity, gain and surface profile to characterize its effect on the electric field in the spatial domain while free-space propagation between optical elements is computed in the spatial frequency domain. Notably, the optical elements can be defined using either theoretical models or experimentally measured data, enabling this method to deliver simulation results closely approximating real-world experimental conditions.

To simplify calculations in the absence of precise disk surface profile measurements, we employed empirical modeling to simulate output beam profiles including radially symmetric aspheric aberrations for each laser configuration. The complex intensity gains[15] for a beam reflected at the disk may be written as follows:

$$G(x,y) = g(x,y)\, e^{i\mathrm{OPD}(x,y)}, \tag{1}$$

where $g(x,y)$ is the gain amplitude accounting for amplification in the pumped region and absorption in the unpumped region (soft-aperture effects) and $\mathrm{OPD}(x,y)$ is the optical phase difference associated with an amplification-reflection at the disk-mirror. The OPD characterizes the effective surface topography of the disk, which includes spherical OPD specified only by dioptric power and aspherical aberration. The aspherical aberration related to the pump profile on the disk surface is assumed to have the form of a step at the edge

https://doi.org/10.1017/hpl.2026.10120 Published online by Cambridge University Press

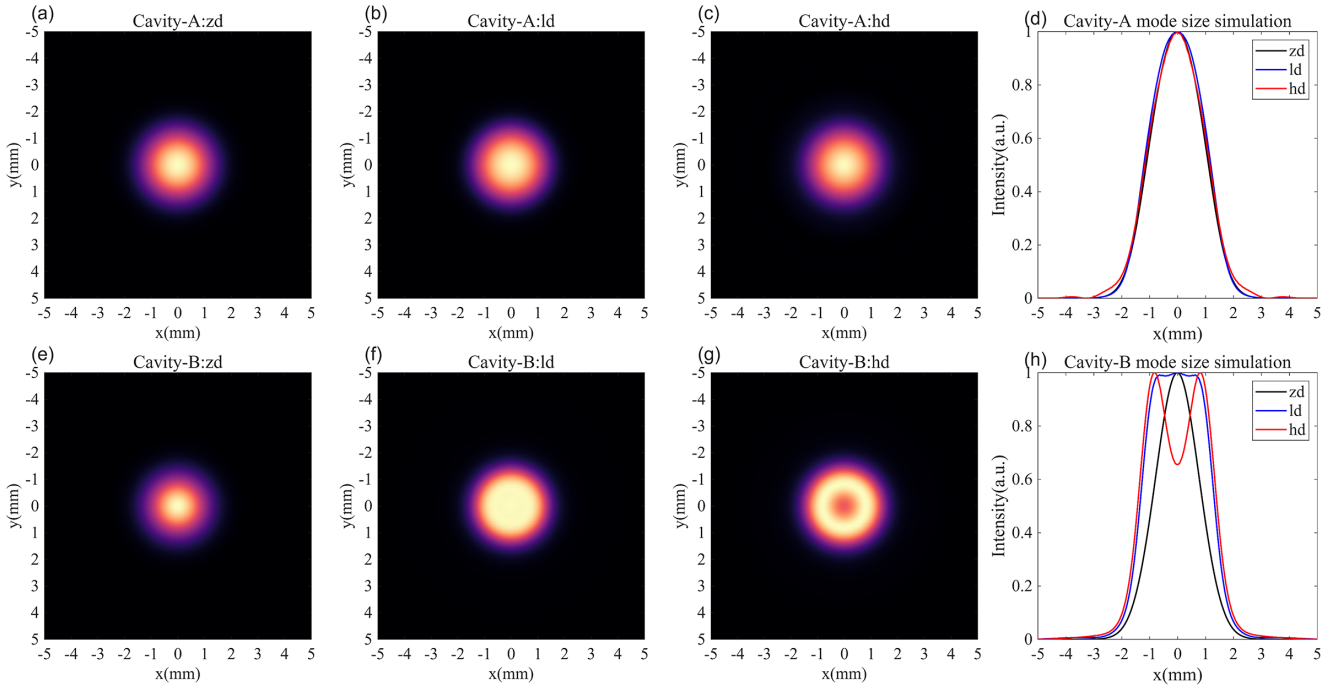


Figure 3. Simulated intensity distributions for different resonator designs. The aberrations are labeled as zero distortion, low distortion and high distortion; the resulting intensity distributions on the laser output (normalized) are shown in (a)–(c) and (e)–(g). The cross-sections of the intensity profiles are compared for various disk aberrations in (d) and (h).

of the pump spot, similar to a Fermi–Dirac distribution[31]:

$$h(r) = \frac{h_0}{1 + \exp\left(\frac{r - r_0}{B_0}\right)}, \tag{2}$$

where h_0 is the height of the top-hat-shaped profile, r_0 is the pump radius, r is the radial coordinate and B_0 is the steepness at the edge of the pump spot. The aberration states are classified according to the height of the top-hat-shaped profile: zero distortion (zd), low distortion (ld) and high distortion (hd). A comparative analysis of the output beam profile evolution under different aspheric aberration levels revealed distinct thermal-induced aberration resistance characteristics between the resonator configurations.

As can be seen from Figure 3, subject to progressive aspheric aberration intensification, Cavity B exhibits sequential transverse mode degeneration: the fundamental Gaussian profile transits to a super-Gaussian distribution at low aberration, ultimately evolving into a doughnut-shaped Laguerre–Gaussian mode under critical distortion amplitudes. In contrast, Cavity A demonstrates robust thermal stability: it maintains a fundamental transverse mode profile with negligible beam size variation under equivalent thermal-induced aspheric aberration conditions. At high aberration levels, beam energy redistributes into diffraction rings. This artifact may originate from boundary diffraction effects inherent in numerical propagation algorithms. In practical optical systems, such diffraction-induced sidelobes would naturally attenuate over propagation distance and may also be filtered via optimized hard-edged apertures. It should be emphasized that incorporating measured disk surface profiles and spatially resolved gain distributions will significantly enhance simulation fidelity in capturing the coupled effects of the disk surface profile and pump effect imprinted onto the intracavity laser beam. These disk surface characterization approaches (e.g., wavefront detection or interferometry) are planned for subsequent investigation. Nevertheless, our simulation results demonstrate the enhanced stability and superior fundamental-mode operation capability of the GESAR configuration. The deliberately increased MPR fully exploits the mode-filtering effect of the gain-induced soft aperture inherent to the crystal, thereby suppressing the high-order mode to maintain robust single-transverse-mode operation.

2.3. *Experimental results and discussion*

For the experimental validation of the described cavity design, both cavities shown in Figure 2 were experimentally constructed and tested by adopting plano-convex mirrors with different radii of curvature. The output beam profiles of each cavity were recorded and analyzed. Simultaneously, the leakage beam profile after intracavity optics was recorded to comprehensively evaluate the transmitted laser spot size for comparison with cavity design specifications. Furthermore, the power-dependent thermal lensing of the disk was incorporated in the cavity design to ensure optimal performance

https://doi.org/10.1017/hpl.2026.10120 Published online by Cambridge University Press

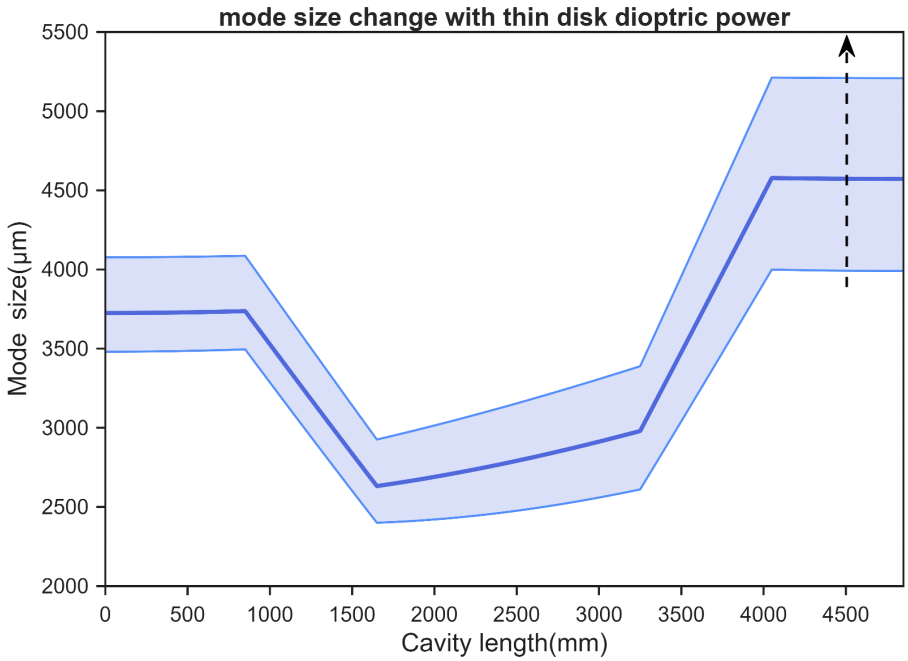


Figure 4. Beam radius of the fundamental mode along the resonator. The arrow direction indicates the increasing disk thermal lensing effect.

under full power operation conditions. In this study, variations in the effective focal length of the thin-disk crystal were measured using resonator stability criteria: by utilizing the critical parameters of the resonator in the stability boundary, the effective focal length of the disk thermal lens can be determined. Through this diagnostic method, we successfully characterized the pump-power-dependent focal shift, revealing a linear dioptric power variation of –0.4 mdpt/W. The cavity was designed such that the mode size on the disk increases with the increasing thermal lensing of the disk, as can be seen from Figure 4. This helps enhance mode discrimination capability according to our simulation.

Experimentally, with the same coupling rate of the output coupler, the two resonator configurations exhibit distinct beam evolution characteristics. Figure 5 shows the measured beam profiles at different pump powers for the two cavities, which demonstrates agreement with the computational predictions. Depending on the operating point, the laser can exhibit Gaussian modes, top-hat modes and doughnut modes for Cavity B, designed using the traditional method, with the MPR of 70%–80% on the disks. The beam quality exhibited progressive degradation with increasing pump power. In contrast, Cavity A, designed by the GESAR method, demonstrates superior thermal stability, maintaining fundamental-mode operation with minimal variation in beam profiles.

To further evaluate the power scaling capability of Cavity A, we incrementally increased the pump power beyond the laser threshold while monitoring the output power and beam profile. The output power as a function of the incident pump power is shown in Figure 6(a). Limited by the available pump power, the maximum output power reached 300 W with a slope efficiency of 49.977% at the average pump power intensity of 2.2 kW/cm^2. Following established power-efficiency growth trends, the output power exhibits potential for further power enhancement through increased pumping intensity.

Besides the power characterization, beam profiles of the linear resonator were recorded as a function of the output power. It can be seen from Figure 6(b) that the intensity beam profiles of the laser output were fundamental mode with typical Gaussian profile across the full power range. With increasing pump power, the linear resonator maintained fundamental-mode (TEM_{00}) operation with a gradual expansion of the beam size up to the maximum output power, while higher-order modes were suppressed successfully. The observed enlargement of the fundamental-mode spot was attributed to enhanced thermal lensing in the disk at higher pump power. Consistent with the resonator design, the fundamental-mode radius as a function of the thermal lens increases. At maximum output power, the beam quality was measured using a beam quality analyzer (Beamage, Gentec-EO). The beam quality factors of $M^2_x = 1.06$ and $M^2_y = 1.15$ indicate near-diffraction-limited performance, as shown in Figure 6(c). The astigmatism may be due to curved optics (thin disk, curved mirrors) being used with a non-zero incidence angle or high-order asymmetric aberrations of the disk laser medium. This consequently indicates that precise disk surface profilometry is essential for reliable performance modeling in practical laser systems – a critical focus of our ongoing research program.

Owing to the QCW pump scheme, the laser output manifested damped relaxation oscillations, presenting multiple

https://doi.org/10.1017/hpl.2026.10120 Published online by Cambridge University Press

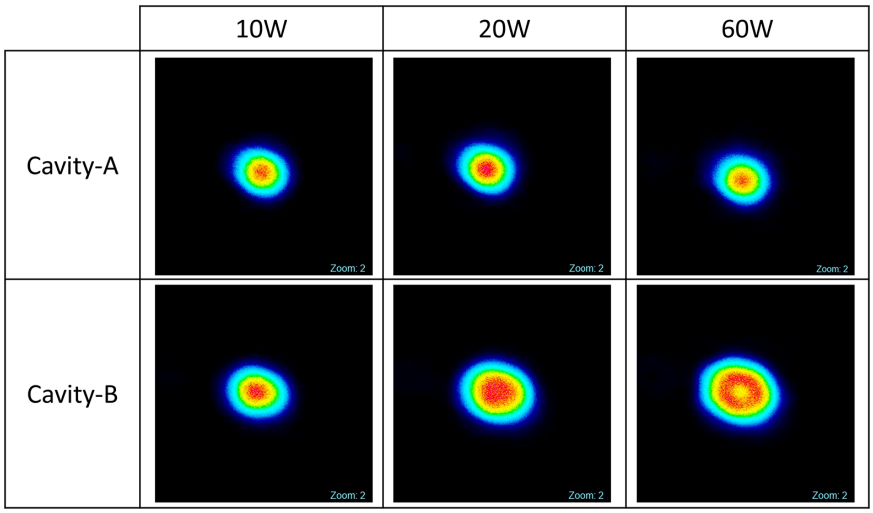


Figure 5. Measured output beam profiles for different resonator designs. The output power is indicated.

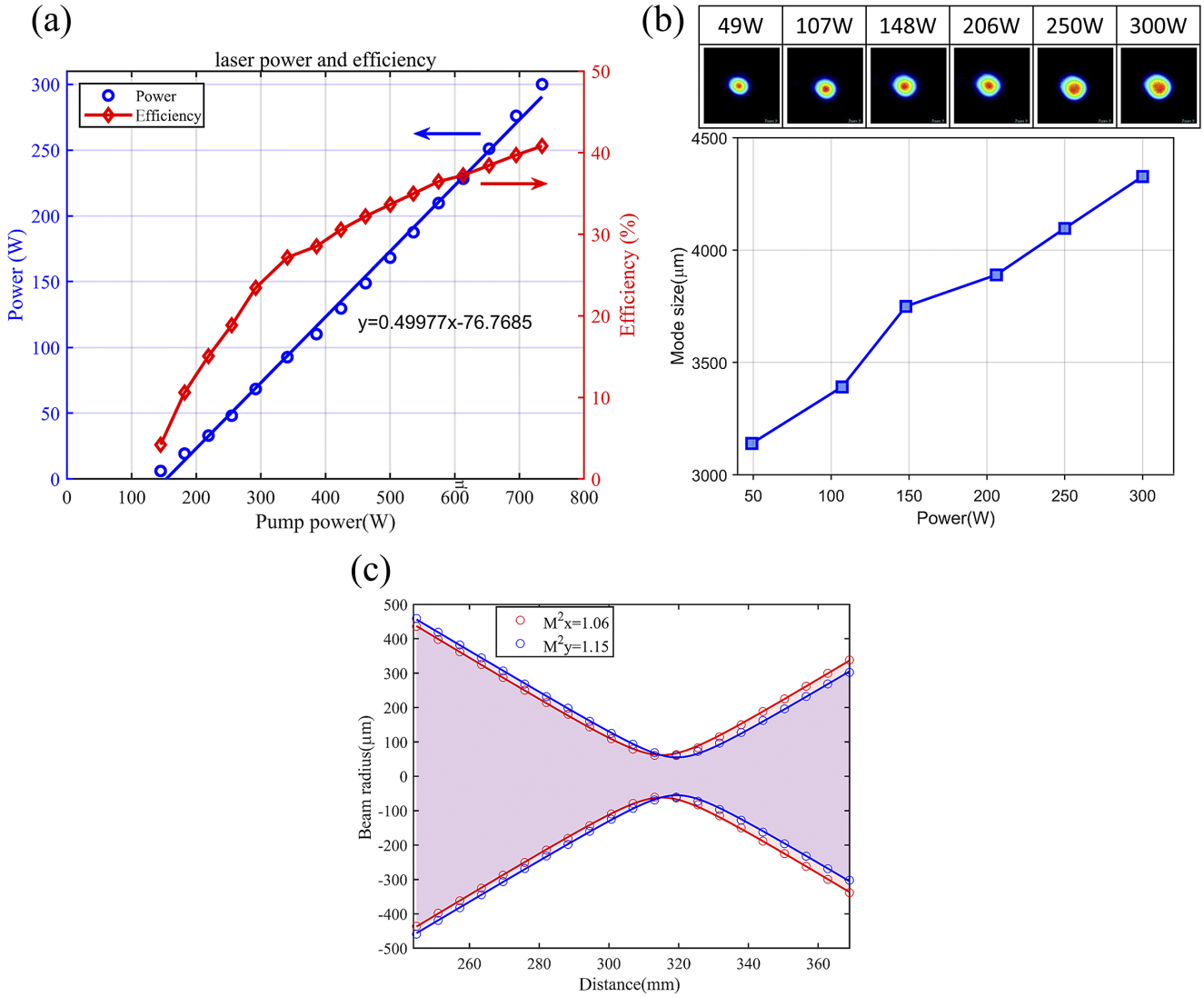


Figure 6. Power characteristics of the thin-disk resonator. (a) Output power and efficiency versus pump power. (b) Beam size and intensity profiles versus output power. (c) Beam quality of the resonator at 300 W.

https://doi.org/10.1017/hpl.2026.10120 Published online by Cambridge University Press

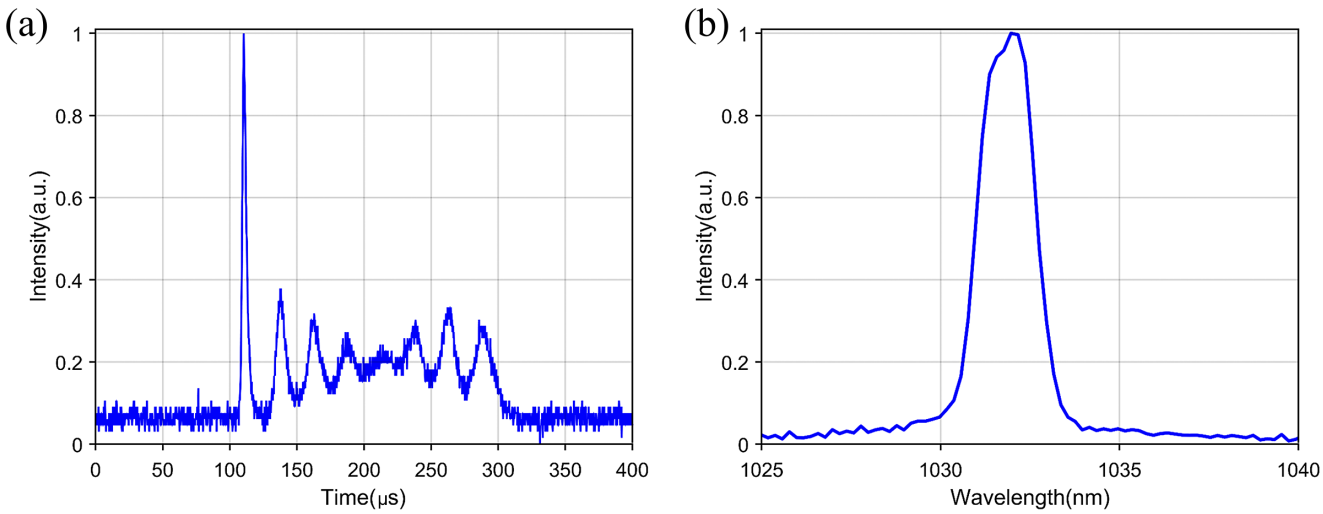


Figure 7. Temporal characteristics of the thin-disk resonator and optical spectrum.

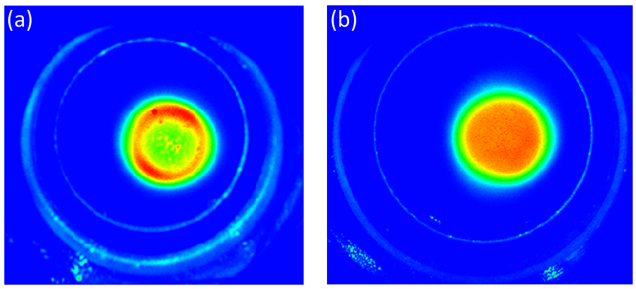


Figure 8. Raw image of the depleted pump spot. (a) On disk 1, the depleted area is less than the pump spot. (b) On disk 2, the extraction region fully covers the pumped area.

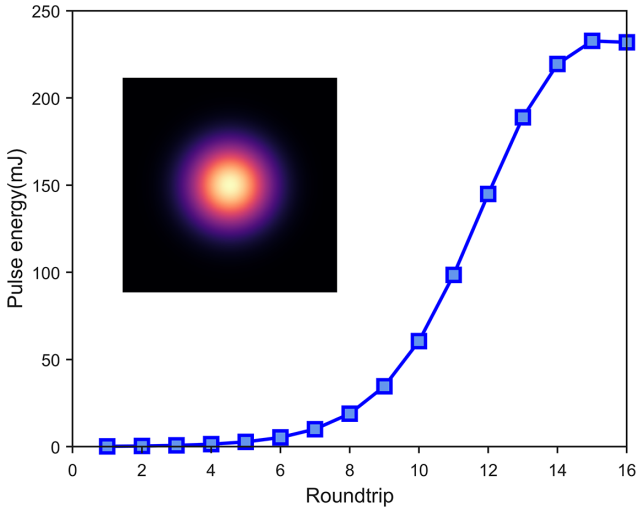


Figure 9. Simulated output pulse energy versus roundtrip and intensity profiles (normalized) of the designed regenerative amplifier.

spikes in its temporal waveform, as shown in Figure 7(a). Moreover, the output laser spectrum had a full width at half maximum (FWHM) of 1.67 nm centered at 1031.86 nm.

Notably, the depleted pump spot image on the disk directly reveals the spatial position and profile of the cavity mode. Figure 8 shows the energy extraction at both thin disks. Due to the inversion depletion by laser amplification in the oscillator, the overlap between the laser mode and the pump spot was visible as a darker region with significantly reduced fluorescence. This reduction in fluorescence clearly indicated the position and profiles of the cavity mode on the disk. On disk 1, the laser mode is smaller than the pump spot, making the extraction zone distinctly visible within the pumped region. On disk 2, the laser mode is designed to be comparable to or larger than the pump spot. As a result, the extraction region fully covered the pumped region, leading to a nearly uniform reduction of fluorescence across the entire pumped region. This observation further validates the effectiveness of our cavity design.

Our thin-disk resonator design demonstrates outstanding thermal stability and fundamental-mode retention capability, effectively suppressing higher-order modes while maintaining a large cavity mode volume. The intrinsic soft aperture of the disk crystal contributes to mode shaping, mitigating the laser performance degradation induced by aspherical aberration. While maintaining a compact cavity geometry with shortened resonator length, this architecture exhibits exceptional thermal alignment stability owing to Fourier transform cavity design. Both numerical simulations and experimental data confirm that power scaling beyond 500 W is achievable through further enlargement of the laser spot size. It also presents an attractive solution for developing regenerative amplifiers operating at the kHz repetition rate with hundred-mJ-level pulse energy. The availability of high-LIDT (laser-induced damage threshold) optics and high-power Faraday rotators has rendered linear resonator architectures a technically feasible alternative. For this purpose, we have designed a regenerative amplifier

https://doi.org/10.1017/hpl.2026.10120 Published online by Cambridge University Press

incorporating dual thin-disk modules. Each module is pumped with a 6.5 mm diameter spot, resulting in a peak power intensity of 6.0 kW/cm^2 under operational conditions of 2 kW peak power at a 1 kHz repetition rate (25% duty cycle). With a seed pulse energy of 100 μJ, numerical simulations of pulse build up and beam profiles confirm that the amplifier can achieve fundamental-mode pulses exceeding 200 mJ at 1 kHz, as illustrated in Figure 9. Experimental validation will be pursued in subsequent studies.

3. Conclusion

We have developed a novel resonator design in which the laser mode size on the disk is strategically enlarged to match or exceed the pump spot. Using a compact resonator with a total length below 5 m, an average output power of 300 W was achieved at a repetition rate of 1 kHz. Through the cavity design optimization, the aspheric aberration of the disk surface can be utilized to generate doughnut-shaped beams or effectively suppressed to ensure fundamental Gaussian beam output. We establish that strategically enlarging the laser spot size on one disk within a dual-disk resonator configuration significantly enhances the soft-aperture mode-shaping effect for higher-order mode suppression, as verified by combined theoretical analysis and experimental data. The GESAR cavity design alleviates the stringent surface profile requirements for high-power fundamental-mode laser disks, making it highly suitable for application in high-power, high-energy thin-disk regenerative amplifiers. It holds great promise for achieving more than 100 mJ pulse energy at kHz-level repetition rates with a compact linear resonator. These advancements represent a significant improvement in system compactness and practicality, facilitating laboratory integration of high-pulse-energy laser systems.

Acknowledgements

This work was supported by the Key Research Program of the Chinese Academy of Sciences (Grant No. PTYQ2022YZ0001) and National Key Research and Development Program of China (Grant No. 2022YFB4601100).

References

1. T. C. Truong, D. Khatri, C. Lantigua, C. Kincaid, and M. Chini, APL Photonics **10**, 040902 (2025).
2. N. Kanda, T. Imahoko, K. Yoshida, A. Tanabashi, A. A. Eilanlou, Y. Nabekawa, T. Sumiyoshi, M. Kuwata-Gonokami, and K. Midorikawa, Light Sci. Appl. **9**, 168 (2020).
3. K. Sugioka and Y. Cheng, Light Sci. Appl. **3**, e149 (2014).
4. H. Guo, J. Xie, G. He, D. Zhu, M. Qiao, J. Yan, J. Yu, J. Li, Y. Zhao, M. Luo, and H. Han, Nano Res. **17**, 6212 (2024).
5. M. Kretschmar, J. Tuemmler, B. Schütte, A. Hoffmann, B. Senfftleben, M. Mero, M. Sauppe, D. Rupp, M. J. J. Vrakking, I. Will, and T. Nagy, Opt. Express **28**, 34574 (2020).
6. B. D. Bruner, R. Maksimenka, N. Thiré, L. Faeyrman, R. Weiss, N. Avni, T. Arusi-Parpar, Y. Pertot, and N. Dudovich, Sci. Rep. **15**, 34438 (2025).
7. C. J. Saraceno, D. Sutter, T. Metzger, and M. A. Ahmed, J. Eur. Opt. Soc. **15**, 15 (2019).
8. A. Giesen, H. Hügel, A. Voss, K. Wittig, U. Brauch, and H. Opower, Appl. Phys. B Lasers Opt. **58**, 365 (1994).
9. T. Dietz, M. Jenne, D. Bauer, M. Scharun, D. Sutter, and A. Killi, Opt. Express **28**, 11415 (2020).
10. C. Herkommer, P. Krötz, R. Jung, S. Klingebiel, C. Wandt, R. Bessing, P. Walch, T. Produit, K. Michel, D. Bauer, R. Kienberger, and T. Metzger, Opt. Express **28**, 30164 (2020).
11. X. Liu, Y. Sui, M. Yuan, G. Zhang, Z. Bai, and Z. Fan, Infrared Phys. Techn. **140**, 105354 (2024).
12. X. Hu, L. Zheng, X. Ma, H. Liu, H. Liu, L. Yan, H. L. Wang, X. Zhu, K. J. Dai, Q. Wang, G. Z. Zhu, Q. Z. Cui, and J. W. Zhang, Laser Photonics Rev. **19**, 2500186 (2025).
13. M. Seidel, L. K. Lang, C. R. Phillips, and U. Keller, Optica **11**, 1368 (2024).
14. S. Xu, Y. Gao, X. Liu, Y. Chen, D. Ouyang, J. Zhao, M. Liu, X. Wu, C. Guo, C. Zhou, Q. Lue, and S. Ruan, High Power Laser Sci. Eng. **12**, e14 (2024).
15. A. Antognini, K. Schuhmann, F. D. Amaro, F. Biraben, A. Dax, A. Giesen, T. Graf, T. W. Hansch, P. Indelicato, L. Julien, C. Y. Kao, P. E. Knowles, F. Kottmann, E. L. Bigot, Y. W. Liu, L. Ludhova, N. Moschuring, F. Mulhauser, T. Nebel, F. Nez, P. Rabinowitz, C. Schwob, D. Taqqu, and R. Pohl, IEEE J. Quantum Electron. **45**, 993 (2009).
16. J. Mende, E. Schmid, J. Speiser, G. Spindler, and A. Giesen, Proc. SPIE **7190**, 71900M (2009).
17. T. Metzger, "High-repetition-rate picosecond pump laser based on an Yb:YAG disk amplifier for optical parametric amplification," PhD. Thesis (Technische Universität Berlin, 2009).
18. J. Neuhaus, D. Bauer, J. Zhang, A. Killi, J. Kleinbauer, M. Kumkar, S. Weiler, M. Guina, D. H. Sutter, and T. Dekorsy, Opt. Express **16**, 20530 (2008).
19. T. Nubbemeyer, M. Kaumanns, M. Ueffing, M. Gorjan, A. Alismail, H. Fattahi, J. Brons, O. Pronin, H. G. Barros, Z. Major, T. Metzger, D. Sutter, and F. Krausz, Opt. Lett. **42**, 1381 (2017).
20. Y. Pfaff, M. Rampp, C. Herkommer, R. Jung, C. Y. Teisset, S. Klingebiel, and T. Metzger, in *Laser Congress 2021* (Optica Publishing Group, 2021), paper AM2A.5.
21. S. Piehler, B. Weichelt, A. Voss, M. A. Ahmed, and T. Graf, Opt. Lett. **37**, 5033 (2012).
22. V. Magni, J. Opt. Soc. Am. A **4**, 1962 (1987).
23. R. Paschotta, Opt. Express **14**, 6069 (2006).
24. A. Siegman, IEEE J. Quantum Electron. **13**, 334 (1977).
25. A. Diebold, F. Saltarelli, I. J. Graumann, C. J. Saraceno, C. R. Phillips, and U. Keller, Opt. Express **26**, 12648 (2018).
26. M. Seidel, L. Lang, C. R. Phillips, and U. Keller, Opt. Express **30**, 39691 (2022).
27. Z. Yao, J. Yu, Y. Chen, J. Sun, Y. Zhang, J. Fan, R. Han, X. Zhang, and F. Chen, Opt. Express **32**, 47041 (2024).
28. Z. Yao, F. Chen, Y. Chen, J. Sun, J. Yu, Y. Zhang, D. Yu, Y. He, K. Zhang, H. Zhou, K. Yang, Z. Zhang, and Q. Wen, Infrared Phys. Techn. **134**, 104855 (2023).
29. Y. Chen, Z. Yao, J. Yu, Y. Zhang, X. Zhang, D. Yu, Y. He, K. Zhang, Q. Pan, J. Sun, and F. Chen, Opt. Laser Technol. **176**, 110875 (2024).
30. A. Alabbadi, M. Larionov, and F. Fink, Opt. Lett. **47**, 202 (2022).
31. D. Blázquez-Sánchez, B. Weichelt, A. Austerschulte, A. Voss, T. Graf, A. Killi, H.-C. Eckstein, M. Stumpf, A. L. Matthes, and U. D. Zeitner, Opt. Lett. **36**, 799 (2011).

https://doi.org/10.1017/hpl.2026.10120 Published online by Cambridge University Press